Craters produced by explosions in a granular medium

F. Pacheco-Vázquez,[1] A. Tacumá,[1] and J. O. Marston[2]
[1]*Instituto de Física, Benemérita Universidad Autónoma de Puebla, Apartado Postal J-48, Puebla 72570, Mexico*
[2]*Department of Chemical Engineering, Texas Tech University, Lubbock, Texas 79409, USA*
(Received 23 May 2017; published 7 September 2017)

We report on an experimental investigation of craters generated by explosions at the surface of a model granular bed. Following the initial blast, a pressure wave propagates through the bed, producing high-speed ejecta of grains and ultimately a crater. We analyzed the crater morphology in the context of large-scale explosions and other cratering processes. The process was analyzed in the context of large-scale explosions, and the crater morphology was compared with those resulting from other cratering processes in the same energy range. From this comparison, we deduce that craters formed through different mechanisms can exhibit fine surface features depending on their origin, at least at the laboratory scale. Moreover, unlike laboratory-scale craters produced by the impact of dense spheres, the diameter and depth do not follow a 1/4-power-law scaling with energy, rather the exponent observed herein is approximately 0.30, as has also been found in large-scale events. Regarding the ejecta curtain of grains, its expansion obeys the same time dependence followed by shock waves produced by underground explosions. Finally, from experiments in a two-dimensional system, the early cavity growth is analyzed and compared to a recent study on explosions at the surface of water.

DOI: 10.1103/PhysRevE.96.032904

Crater formation is a fundamentally important topic in geophysics and planetary science motivated by the observation of craters on Earth and some of our nearby neighbors (i.e., our moon and Mars). Today, we know that most of the craters were produced by the impact of meteorites.

One consistent line of inquiry has been to derive the energy involved in the formation of a given crater [1–4], which has led to many inverse problem studies, ranging from laboratory scale experiments with steel spheres where $D \sim O(10^{-1})$ m and $E_0 \sim O(10^{-3})$ J up to meteor craters with $D \sim O(10^3)$ m and $E_0 = O(10^{16})$ J. It has been proposed that a scaling law relating crater diameter to the energy of the impact, $D \sim E_0^{1/4}$, is valid in this energy range, however this upper energy limit is based only on a single, loosely constrained data point and has not yet been validated. In fact, high-velocity studies have revealed scaling laws with significantly lower exponents for the crater size in terms of the impact energy [5–7], therefore casting doubt on the universality of a single exponent. For typical impact experiments, the ejecta velocities (e.g., [8–10]), crater diameter (e.g., [2,11]), and penetration depth of the projectile (e.g., [12–15]) are the characteristic measurements taken. For authoritative details on this topic, the reader is referred to Refs. [7,16–20].

With the exception of recent studies of cavity collapse [21,22], other cratering studies generally pertain to near-surface explosions [23–26]. In this phenomenon, the point-source release of energy excavates material to form a crater, and dimensional analysis predicts linear crater dimensions to scale as $W^{1/3}$, where W is the weight (or energy) of the explosive charge. This scaling failed across a broad range of data due to factors such as eject fallback and material heterogeneity [27], and an empirically derived constant of 0.3 has been proposed [23]. In fact, depending on the variables included in the dimensional analysis, all scaling laws are shown to be bounded by cube root and quarter root rules [23,28].

So far, most craters generated by explosions are studied at a large energy scale ($> 10^6$ J) with only a handful of reports at the laboratory scale (see, e.g., [29–31]). Here we report on small explosions ($\sim 10^2$ J) at the surface of a model three-dimensional granular bed, and also in a two-dimensional cell that allows us to observe and analyze the cavity growth dynamics. The best-fit relation between crater dimensions and energy is determined and compared with large-scale results. In particular, we discuss some morphological features that distinguish craters created by explosions from craters with other origins.

I. EXPERIMENTAL SETUP

A granular bed was prepared in a cylindrical container (height 40 cm and diameter 60 cm), comprised of 180 μm Oklahoma silica sand particles ($\rho_s = 2.6$ g/cm^3). The bed is prepared in a similar fashion to that described in [22] to yield a consistent initial solids packing fraction of $\phi \approx 0.59 \pm 0.01$. A small explosive device is then placed directly in the center of the bed and buried so that the top of the device is at the same level of the granular surface. The device itself is a 1 cm^3 hollow metallic cylinder of 10 mm height and with a 3 mm diameter hole at the top used to fit the fuse that ignites explosive powder confined within the metallic chamber. The powder was obtained from firecrackers and measured out in specified masses ranging from 0.1 to 0.6 g on a balance with a tolerance of ± 0.005 g. The bottom of the chamber (facing into the granular bed) is open, but covered with paper layers so that the initial blast is directed vertically down into the bed. The approximate energy released by the deflagration of the powder, for which the principal constituent is potassium nitrate (KNO_3), is 3 MJ/kg, in which case we can specify the approximate energy E_0 as 300–1800 J. Only a reduced fraction of this energy is used to produce the resulting crater, while the rest is mainly dissipated as heat. The events were captured with a high-speed video camera (Photron Fastcam Mini UX100) at frame rates up to 20 000 fps, while the crater shapes and dimensions were captured by laser profilometry after the explosion. The underground cavity growth dynamics

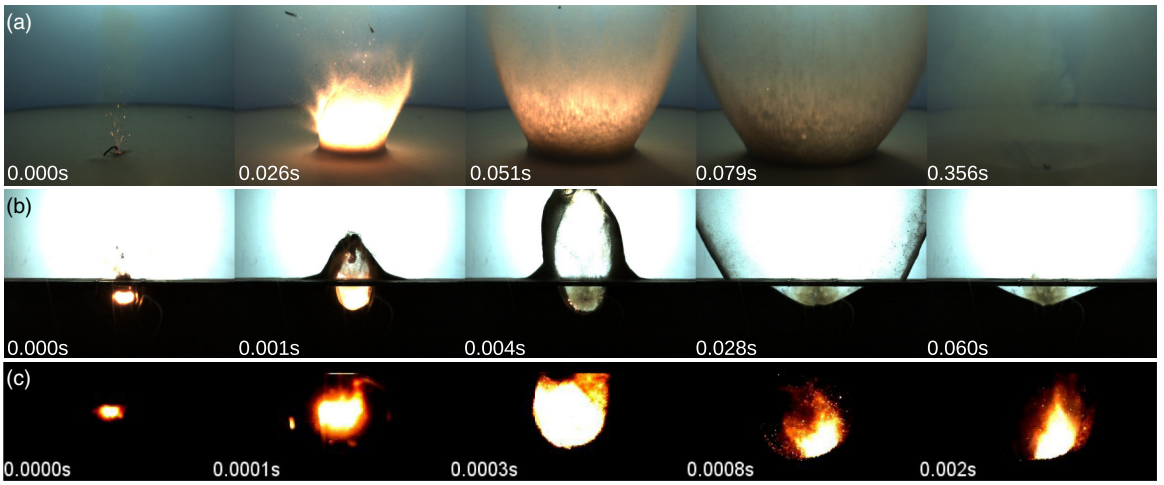

FIG. 1. Explosions in granular media: Snapshots taken from high-speed video sequences of (a) an explosion in a 3D bed setup with $m = 0.4$ g, (b) an explosion in a quasi-two-dimensional (2D) cell with $m = 0.2$ g, and (c) early cavity growth in the 2D cell for $m = 0.2$ g, recorded at 20 000 fps. See also the supplemental videos [32].

following the explosion was visualized using a pseudo-two-dimensional setup fabricated from acrylic plates ($35 \times 50\,\mathrm{cm}^2$) separated by $w = 1.5$ cm spacers. Only the smaller explosives were used in this system to avoid container damage, and the walls were strengthened with an aluminum frame to inhibit cell expansion during the explosion.

II. CRATER MORPHOLOGY

Illustrative image sequences of three-dimensional (3D) and 2D experiments are shown in Figs. 1(a) and 1(b), respectively. The ignition corresponds to $t = 0$. The explosion first produces an underground cavity, then the material is expelled outside generating an ejecta curtain, and finally a crater forms at the surface. Figure 1(c) shows that the explosion itself lasts less than 1 ms. During this short time, a shock wave generated by the explosion accelerates the mass of sand violently and gives rise to a cavity and a raised rim below and above the surface, respectively. High-speed videos of the cratering process in 3D and 2D systems can be found in the supplementary information [32].

Figure 2(a) shows a typical crater produced by an explosion and an example of the raw image for the laser profilometry. Analysis of these images yields discrete data points, which we first fit to an equation before performing a solid of revolution to obtain the crater volume. The best fit to the data is given by the equation of a hyperbola:

$$z(x) = H - a + (a^2 + x^2 \tan^2\theta)^{1/2},$$

where H is the maximum crater depth measured at $x = 0$, a is a fitting parameter with $O(1\text{ cm})$, and θ is the acute angle between the lateral wall asymptotes and the horizontal plane. The results of this fitting procedure are shown in Fig. 2(b) (solid lines) in the x-z plane for different values of explosive mass, m. In nearly all cases, the profiles are almost conical with slopes $\theta \sim 16^\circ$–20°, less than the angle of repose of this granular material, $\theta_R = 32.5^\circ$.

From these profiles, we can also measure the crater diameter D given by the distance between the lateral walls at the initial surface level, and we calculate the mean crater aspect ratio $\alpha = D/H = 7.2 \pm 0.4$ [Fig. 2(c)]. With reference to Fig. 2(d), we note that the raised rim height H_{rim} increases almost linearly with the energy of the explosion. The only other cratering

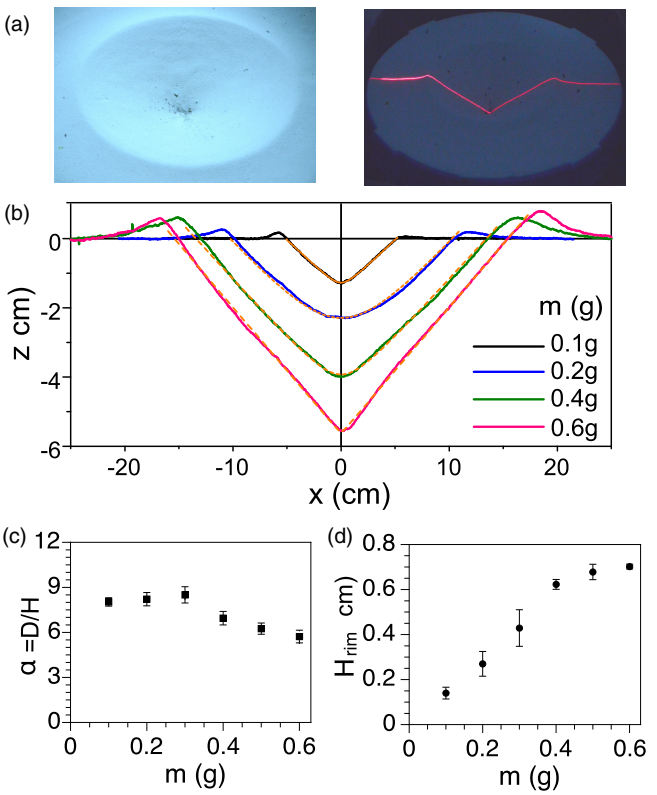

FIG. 2. (a) Crater produced by an explosive with $m = 0.4$ g of gunpowder, and its surface profile obtained with a laser line. (b) Crater profiles produced by different explosive masses m (solid lines). Craters have raised rims and a hyperbolic shape approaching almost a conical depression (dashed lines). (c) The crater aspect ratio $\alpha = D/H$ is nearly independent of m, although it decreases slightly for larger values of m. (d) Rim height H_{rim} measured from $z = 0$ as a function of m.

TABLE I. Summary of the morphological properties of craters produced by different mechanisms at laboratory scale, according to some experimental investigations and the results reported in this research (a blank space means "not quantified").

Origin	Ref.	Profile/technique	Scaling	$H_{\rm rim}$	$\alpha = D/H$	Remarks
Impact (solid projectiles)	[2]	Bowl-shaped (observed with the naked eye)	$D \propto E^{1/4}$ $H \propto E^{1/4}$		∼8.4	Craters with central uplifts and terraces at higher energy α increase at higher energies.
	[3]	Hyperboloid (laser prof. and fit)	$D \propto E^{1/4}$ $H \propto E^{1/5}$	Independent of E	∼6–15	$H_{\rm rim}$ is fixed by the projectile radius. α is independent of E and fixed by the ball size.
	[14]		$D \propto E^{1/4}$			D and H are separate lengths set by separate physics. H is related to the stopping force on the ball.
	[39]	With central uplifts (laser profilometry)		Increases with ϕ		Crater shape and displaced material are sensitive to ϕ. Large central peaks and deeper craters at small ϕ.
Impact (granular projectiles)	[11]	Bowl-shaped (cross-sectional view)	$D \propto E^{1/4}$ $H \approx$ const		$\propto E^{1/4}$	Projectiles are pulverized by the impact. H fixed by ball cohesive strength and target properties. Craters with central uplift appear when E is increased.
Subsidence	[21]	Hyperboloid (laser profilometry)		No raised rim	$\sim 5 \pm 2$	Collapse of small cavities produced by removing a cylinder from a bed of beads. No corona, central uplift.
Collapse of pressurized cavities	[22]	Spherical bowl-shaped (shadow projection)	$D \propto V^{1/3}$ $H \propto V^{1/3}$	No raised rim	$\sim 7 \pm 1$	D and H are determined by the initial cavity volume V. Large cavities produce jets and crater with central uplift The corona collapses inside the cavity.
Explosions	[29]	Bowl-shaped at $s = 0$ to conical at $s \approx 1$ cm (profilometry)			∼4 but it increases with s.	Impact crater simulated with an explosion at a certain depth, proved only for 0.150 g of PETN (870 J) placed at different depths s.
	[30]	Bowl-to-conical (cross sectional view).				Performed in 3D and quarter-space tests container. Morphological features are only described, and approximated illustrations based on videos are reported.
	[31]	Bowl-shaped (cross-sectional view)				V, D, H, ejecta of grains, material stress, and strain were measured for different charges. Experiments performed in 3D and quarter-space tanks.
	See text	Hyperboloid nearly conical (laser profilometry and fit)	$D \propto E^{0.30}$	$\propto E$	∼7	Corona spreads outside the cavity and central uplifts never appear. $H_{\rm rim}$ grows linearly with E. Experiments in 3D and 2D systems. Analysis of ejecta curtain and cavity growth dynamics.

process leading to hyperbolic craters with raised rims is for the impact of solid projectiles [2,3], but in such cases $H_{\rm rim}$ is found to be independent of the impact energy. Craters produced by projectiles that fragment on impact are nearly parabolic [11], as are meteor craters, while craters produced by the collapse of underground cavities have similar aspect ratios but with a dome-shaped geometry and a flat rim [22] for pressurized cavities, and they are hyperbolic but also without raised rims for nonpressurized cavities [21]. In pioneering reports of laboratory-scale explosions, it is mentioned that conical craters are produced in dry sand, whereas more complex morphologies, including central mounds, concentric rings, and terraces, occurred in cemented sand [30,31]. A summary of the morphology of craters produced by different mechanisms in small-scale experiments is presented in Table I. Note that a quantitative analysis of some of the features and the scaling laws for explosion cratering at laboratory scale were missing before the present research.

III. SCALING LAWS

From dimensional analysis (e.g., [23–26]), one expects the linear dimensions (depth and diameter) to scale as $H, D \sim E_0^{1/3}$, so that $V \sim D^2 H \sim E_0 \propto m$. To test this hypothesis,

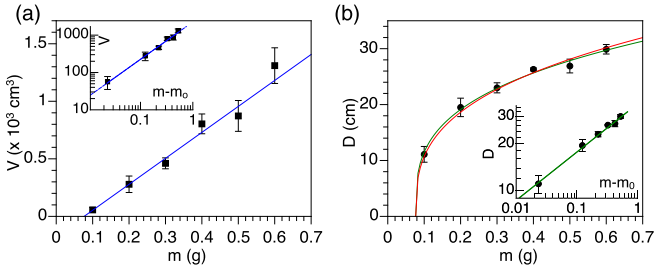

FIG. 3. (a) Crater volume V as a function of mass m. The linear fit predicts $m_0 \approx 0.076$ g. (b) Crater diameter D vs m. The log-log plot (inset) reveals a power-law $D = A(m - m_o)^{0.30}$.

we used the surface profile to calculate the crater volume V from the equation of a hyperboloid given by

$$V = \frac{1}{6}\left(\frac{3D^2}{4H^2} - \frac{1}{\tan^2\theta}\right)\pi H^3.$$

Indeed, Fig. 3(a) shows that V follows a linear relation with m (note the $\log_{10}$-$\log_{10}$ inset indicates an exponent of 0.97 ± 0.04). In particular, the best linear fit intercepts the x axis at $m = m_0 = 0.076 \pm 0.02$ g, which corresponds to $V = 0$ and physically represents the minimum mass to break the combustion chamber. To confirm this, we performed several experiments with $m = 0.050$ g, and in most occasions the powder burned inside the chamber without generating an explosion.

Figure 3(b) shows the crater diameter D as a function of the explosive mass m. Following from the scaling analysis, the data (black points) could be reasonably well described by a 1/3-power law (red line), but the best fit, as determined by the correlation coefficient, is a 0.3-power law (green line) of the form $D = A(m - m_0)^p$, where $m_0 = 0.076$ g and $p = 0.305 \pm 0.016$. This smaller exponent was the subject of detailed analysis by [23] and empirical scaling [27] across different scales. The fact that the same power-law exponents apply here at the laboratory scale is an indication of the universality of scaling of explosive crater formation, at least for surface explosions. Moreover, since the material is systematically prepared before the explosion, the deviation from the 1/3 rule is not related to medium inhomogeneities, as was previously assumed [27].

IV. EJECTA CURTAIN

Let us now describe some of the dynamical features during the crater formation. Following the explosion, the material around the ignition point is ejected radially forming a corona that expands until collapsing outside the cavity. Figure 4(a) shows the corona diameter measured at surface level, $D_{\rm cor}$, as a function of time for different values of m. The $\log_{10}$-$\log_{10}$ plot in Fig. 4(b) indicates a power-law dependence given by $D_{\rm cor} \propto (m - m_0)^{1/3} t^{0.30}$. The same dependence ($\propto t^{0.30}$) was found in underground explosions [33] by monitoring the expansion of the shock wave. This concordance shows that the initial curtain expansion is a good proxy for the cavity growth and estimating the explosive energy.

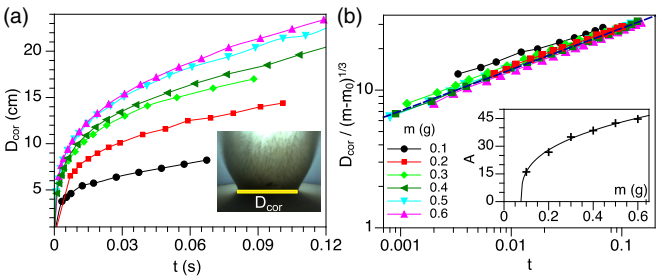

FIG. 4. (a) Corona growth in 3D explosions for different values of m. (b) $D_{\rm cor}$ measured at the surface level as a function of time follows a growth power law $D_{\rm cor} = At^{0.30}$, with $A = (56.1 \pm 0.5)(m - m_0)^{1/3}$ determined in the inset.

V. EARLY CAVITY GROWTH

The quasi-2D system was used to visualize the underground cavity expansion following the explosion. The cavity radii, $R_{\rm cav}$, as a function of t derived from the videos for different values of m are shown in the inset of Fig. 5(a) (color points). In the main plot, the case $m = 0.2$ g is used as an example to compare the experiment with different models discussed below.

In Ref. [34], the early cavity growth produced by an explosion at the water surface was described with a potential flow model simplifying to the expression for the radius $R^3\dot{R}^2 = E_0/\rho$, which easily yields the result $R(t) \propto t^{2/5}$ (here we used indistinctly $R_{\rm cav} = R$). This 2/5 scaling law was established by Taylor for shock wave propagation following a nuclear blast [35], and it was also found during excitation of hard spheres by examining the growth rate of particle collisions in 2D and half-space simulations [36]. Nevertheless, the model considers that the overpressure generated by the explosion relaxes to ambient on a millisecond time scale, shorter than the expansion time of the cavity [$t \sim O(10^{-1}$ s)]. Here we modify the potential flow model by considering the pressure drop from an initial value, P_i, to ambient, P_0, for an isothermal expansion of the quasi-2D cavity during the observed time $t \approx O(10^{-3}$ s) and adding a viscous term to include the dissipative nature of the granular medium [37,38]. Under these conditions, the

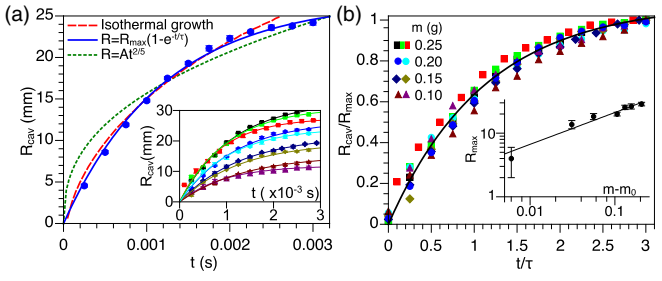

FIG. 5. (a) Inset: $R_{\rm cav}$ vs t in 2D explosions for different masses. Main plot: the case $m = 0.2$ g (solid points) is compared with three models: $R_{\rm cav} = R_{\rm max}(1 - e^{-t/\tau})$ (solid lines), isothermal model (red dashed line), and power-law model $R(t) = At^{2/5}$ (green dotted line). (b) $R_{\rm cav}/R_{\rm max}$ vs t/τ. The heuristic model describes fairly well the growth process with the average value $\tau = 1.127$ ms. The inset shows that $R_{\rm max} \propto (m - m_0)^{1/2}$.

differential equation for the cavity dynamics is

$$R\ddot{R} + \frac{3}{2}\dot{R}^2 + 4\mu\frac{\dot{R}}{R} = \frac{P_i\left(\frac{R_i}{R}\right)^2 - P_0}{\rho},$$

where μ is a free parameter, $P_i = O(10^9$ Pa), and $R_i = O(10^{-4}$ m). As shown in Fig. 5(a), the numerical solution of the above equation (dashed line) approaches better the experimental measurements than $R(t) \propto t^{2/5}$ (dotted line), but a considerable discrepancy still exists. The best data fit (blue line) is given by the heuristic equation:

$$R(t) = R_{\max}(1 - e^{t/\tau})$$

with τ a characteristic time. This equation is also plotted in the inset of Fig. 5(a) (color lines) for different values of m, with excellent agreement in all cases.

If we consider that the mass of grains displaced by the cavity formation is proportional to the energy released during the explosion E_0, then $M_{\text{cav}} = \rho\pi R_{\max}^2 w \propto E_0$, where $\rho = 2.66 \pm 0.05$ g/cm^3 is the density of sand. Since the explosion is radially symmetric, inertial effects are considerably greater than gravitational effects, and M_{cav} is in turn proportional to the effective mass of the explosive. Then, one finds $R_{\max} = \kappa[(m - m_0)/w\rho\pi]^{1/2}$, where κ is a dimensionless constant of proportionality. Accordingly, the $\log_{10}$-$\log_{10}$ plot shown in the inset of Fig. 5(b) shows that $R_{\max}$ is well fitted by a power law of $(m - m_0)^{1/2}$ with $\kappa = 236.8 \pm 18.3$. Using $R_{\max}$ to normalize R_{cav}, it is found that the cavity growth collapses according to $R_{\text{cav}}/R_{\max} = (1.08 \pm 0.01)(1 - e^{-t/\tau})$, as shown in Fig. 5(b), where $\tau = 1.127 \pm 0.037$ ms is the average of the characteristic times of the individual fits shown in the inset of Fig. 5(a). Therefore, the cavity growth velocity $dR/dt = (R_{\max}/\tau)e^{-t/\tau}$ gives initial maximum velocities of $O(10^2)$ m/s.

It is interesting to note that explosions at the free surface of water [34] exhibited the same scaling exponent for maximum cavity size versus energy, i.e., $R_{\max} \sim E_0^{1/4}$, as for impact cratering. However, in the granular bed, we found $R_{\max} \propto (m - m_o)^{0.30} \sim E_0^{0.3}$ as found in large-scale events. In contrast, the scaling obtained in the quasi-2D system was $R_{\max} \propto E_0^{1/2}$, which is related to the confinement effects due to the lateral walls.

VI. CONCLUDING REMARKS

Hyperbolic craters with raised rims result from surface level explosion in a granular bed. Our results here are the first laboratory-scale craters from surface explosions where the mass has been systematically varied. Our observations indicate that the established 0.3 power-law scalings for large craters hold across many orders of magnitude of E_0, however a broader parameter range needs to be considered at the laboratory scale to rule out the 1/3-scaling law from dimensional analysis. This caveat notwithstanding, crater formation by explosions exhibits universality. By comparing the geometry of craters by diverse mechanisms and the finer features such as rim energy dependence, we postulate that profilometry may help to classify craters observed on earth, lunar, and planetary surfaces, although caution should be used because impact craters can be very similar to explosion craters under certain conditions. Finally, we note that for our experiments we considered a relatively loose packing ($\phi \approx 0.59$) and quasispherical grains. Performing a systematic variation of packing and grain shape could provide a robust test of the crater volume scaling found here. Also, testing established scaling laws ($t^{2/5}$) for the growth rate of shock waves and particle-collision zones in different configurations (experiment versus simulation, quarter-space versus half-space, etc.) would be of interest.

ACKNOWLEDGMENTS

We thank Brandon Weeks and S. Hidalgo-Caballero for helpful discussions on the explosives and the isothermal model, respectively. F.P.V. and A.T. thank CONACYT Mexico Project No. 242085 of the Sectoral Research Fund for Education, and VIEP-Project 2017. J.M. thanks TTU for financial support.

[1] H. J. Melosh, *Impact Cratering: A Geologic Process* (Oxford University Press, New York, 1989).
[2] A. M. Walsh, K. E. Holloway, P. Habdas, and J. R. de Bruyn, Phys. Rev. Lett. **91**, 104301 (2003).
[3] S. J. de Vet and J. R. de Bruyn, Phys. Rev. E **76**, 041306 (2007).
[4] D. R. Dowling and T. R. Dowling, Am. J. Phys. **81**, 875 (2013).
[5] D. E. Gault and J. A. Wedekind, *Experimental Hypervelocity Impact into Quartz Sand-II: Effects of Gravitational Acceleration* (Pergamon, New York, 1977).
[6] H. Mizutani, S.-I. Kawakami, Y. Takagi, and M. Kumazawa, J. Geophys. Res. **88**, 835 (1983).
[7] K. A. Holsapple, Annu. Rev. Earth Planet. Sci. **21**, 333 (1993).
[8] W. K. Hartmann, Icarus **63**, 69 (1985).
[9] J. E. Colwell, S. Sturke, M. Cintala *et al.*, Icarus **195**, 908 (2008).
[10] J. O. Marston, E.-Q. Li, and S. T. Thoroddsen, J. Fluid Mech. **704**, 5 (2012).
[11] F. Pacheco-Vázquez and J. C. Ruiz-Suárez, Phys. Rev. Lett. **107**, 218001 (2011).
[12] K. A. Newhall and D. J. Durian, Phys. Rev. E **68**, 060301(R) (2003).
[13] J. R. de Bruyn and A. M. Walsh, Can. J. Phys. **82**, 439 (2004).
[14] J. S. Uehara, M. A. Ambroso, R. P. Ojha, and D. J. Durian, Phys. Rev. Lett. **90**, 194301 (2003).
[15] H. Katsuragi and D. J. Durian, Nat. Phys. **3**, 420 (2007).
[16] J. D. O'Keefe and T. J. Ahrens, Icarus **62**, 328 (1985).
[17] K. R. Housen and K. A. Holsapple, Icarus **211**, 856 (2011).
[18] J. C. Ruiz-Suarez, Rep. Prog. Phys. **76**, 066601 (2013).
[19] H. Katsuragi, *Physics of Soft Impact and Cratering* (Springer, Tokyo, 2016).
[20] D. Van der Meer, Annu. Rev. Fluid Mech. **49**, 463 (2017).
[21] S. J. de Vet and J. R. de Bruyn, Granular Matter **14**, 661 (2012).

[22] F. E. Loranca-Ramos, J. L. Carrillo-Estrada, and F. Pacheco-Vázquez, Phys. Rev. Lett. **115**, 028001 (2015).
[23] A. J. Chabai, J. Geophys. Res. **70**, 5075 (1965).
[24] L. J. Vortman, J. Geophys. Res. **73**, 14 (1968).
[25] R. M. Schmidt and K. R. Housen, Int. J. Impact Eng. **5**, 543 (1987).
[26] R. D. Ambrosini, B. M. Luccioni, R. F. Danesi, J. D. Riera, and M. M. Rocha, Shock Waves **12**, 69 (2002).
[27] US Army Engineer Waterways Experiment Station, Technical Report No. 2-547 (1961).
[28] K. A. Holsapple and R. M. Schmidt, J. Geophys. Res. **85**, 7247 (1980).
[29] V. R. Oberbeck, J. Geophys. Res. **76**, 5732 (1971).
[30] A. J. Piekutowski, in *Proceedings of the 11th Lunar and Planetary Science Conference* (Pergamon, New York, 1980), pp. 2129–2144.
[31] A. J. Piekutowski, *Impact and Explosion Cratering* (Pergamon Press, New York, 1977), pp. 67–102.
[32] See Supplemental Material at http://link.aps.org/supplemental/10.1103/PhysRevE.96.032904 for videos of explosions at the surface of three-dimensional and two-dimensional granular beds.
[33] O. S. Kolkov, A. M. Tikhomirov, and A. F. Shatsukevich, Fiz. Goren. Vzryv. **3**, 569 (1967).
[34] A. Benusiglio, D. Quere, and C. Clanet, J. Fluid Mech. **752**, 123 (2014).
[35] M. A. B. Deakin, Int. J. Math Ed. Sci. Tech. **42**, 1069 (2011).
[36] T. Antal, P. L. Krapivsky, and S. Redner, Phys. Rev. E **78**, 030301(R) (2008).
[37] J. J. Stickel and R. L. Powell, Annu. Rev. Fluid Mech. **37**, 129 (2005).
[38] Y. Forterre and O. Pouliquen, Annu. Rev. Fluid Mech. **40**, 1 (2008).
[39] P. Umbanhowar and D. I. Goldman, Phys. Rev. E **82**, 010301(R) (2010).